Synthesis, Characterization, and Activity Evaluation of $DyVO_4/g-C_3N_4$ Composites under Visible-Light Irradiation

ARTICLE *in* INDUSTRIAL & ENGINEERING CHEMISTRY RESEARCH · NOVEMBER 2012

Impact Factor: 2.59 · DOI: 10.1021/ie301774e

7 AUTHORS, INCLUDING:

Yiming He
Zhejiang Normal University
76 PUBLICATIONS **761** CITATIONS
SEE PROFILE

Mengfei Luo
Zhejiang Normal University
75 PUBLICATIONS **1,267** CITATIONS
SEE PROFILE

I&EC research
Industrial & Engineering Chemistry Research

Article

pubs.acs.org/IECR

Synthesis, Characterization, and Activity Evaluation of $DyVO_4$/g-C_3N_4 Composites under Visible-Light Irradiation

Yiming He,*[,†] Jun Cai,[†] Tingting Li,[‡] Ying Wu,[‡] Yanmin Yi,[§] Mengfei Luo,[‡] and Leihong Zhao[‡]

[†]Department of Materials Physics and [‡]Institute of Physical Chemistry, Zhejiang Key Laboratory for Reactive Chemistry on Solid Surfaces, Zhejiang Normal University, Jinhua, 321004, China

[§]Center Station of Suzhou Environmental Monitoring, Suzhou, 215004, China

Supporting Information

ABSTRACT: $DyVO_4$/graphitic carbon nitride ($DyVO_4$/g-C_3N_4) composite photocatalyst with visible-light response was prepared by a milling and heating treatment method. The synthesized powder was characterized by X-ray diffraction, thermogravimetry/differential thermal analysis, N_2 adsorption, Fourier transform infrared spectroscopy, X-ray photoelectron spectroscopy, scanning electron microscopy, transmission electron microscopy, and UV−vis diffuse reflection spectroscopy. The activity of composite photocatalyst $DyVO_4$/g-C_3N_4 for photodegradation of rhodamine B is much higher than that of either single-phase g-C_3N_4 or $DyVO_4$. The obviously increased performance of $DyVO_4$/g-C_3N_4 is mainly ascribed to the electron−hole separation enhancement at the interface of the two semiconductors, as proven by photoluminescence spectroscopy and photocurrent measurement. In addition, it is found that holes and $^{\bullet}O_2^-$ are the main active species in the photocatalytic oxidation of RhB solution in the presence of $DyVO_4$/g-C_3N_4 composite.

1. INTRODUCTION

Decomposition of water and removal of environmental pollutants through photocatalytic reaction has drawn increasing attention over the last few decades.[1−3] Because of its high activity and chemical stability, TiO_2 has been known as the most efficient photocatalyst.[4] However, considering the application in practice, a photocatalyst should also have the characteristics of low cost and visible-light response. TiO_2 can only absorb ultraviolet (UV) light, which occupies no more than 4% of the solar spectrum, because of its large band gap, which limits its application. Several approaches have been reported to extend the light response of TiO_2. These approaches include the incorporation of metal ions (Fe^{3+}, V^{5+}, W^{6+})[5,6] or nonmetal ions (C^{4-}, N^{3-}, S^{2-})[7,8] into the lattice of TiO_2, the introduction of oxygen vacancies into the lattices of TiO_2,[9,10] the dye sensitization of TiO_2,[11] and the combination of TiO_2 with a semiconductor with a small band gap.[12,13] However, the activities of these materials under visible-light irradiation are limited. Meanwhile, some researchers are devoted to explore non-TiO_2 semiconductor materials. Many novel semiconductor photocatalysts were reported, such as $BiVO_4$, Ag_3PO_4, and $CaBi_6O_{10}$.[14−16] However, these novel materials still suffer from the problems of low photocatalytic activity, instability, high cost, and so on. The developing of an efficient photocatalyst under visible light is still desired.

Graphitic carbon nitride (g-C_3N_4) is a metal-free semiconductor that has the characteristics of high thermal and chemical stability and versatile optical, electronic, tribological, and catalytic properties. These unique properties make g-C_3N_4 a valuable material in various potential applications, such as gas storage, the conversion of solar light into electricity, and the synthesis of superhard carbon nitride materials.[17−19] Wang et al. first reported in 2009 that g-C_3N_4 has photocatalytic activity in the production of hydrogen or oxygen during water splitting under visible-light irradiation.[20] Yan et al. then reported that metal-free g-C_3N_4 has good performance in the photodegradation of organic pollutants.[21] This indicates that the metal-free g-C_3N_4 also has promising potential in the photocatalysis field.[22] However, g-C_3N_4 suffers from the disadvantages of low surface area and low quantum efficiency, both of which limit its photocatalytic performance. Therefore, many attempts have been made to improve the photocatalytic performance of g-C_3N_4, such as noble metal deposition,[23] nonmetal doping,[24] preparation of nano/porous g-C_3N_4,[25,26] protonating g-C_3N_4 by strong mineral acids,[27] and constructing a heterojunction composite with another semiconductor.[28−33] The last approach is commonly used because the coupling of another semiconductor could not only offer the driving forces to separate and transfer photogenerated electron−hole pairs but also extend the light response of the photocatalyst. For example, Yan et al. prepared g-C_3N_4/TaON composite with higher activity than either a single phase of g-C_3N_4 or TaON in RhB photodegradation.[28] The increased performance is mainly ascribed to the enhancement of electron−hole separation in the semiconductors. Lei et al. reported that the coupling of Bi_2WO_6 with g-C_3N_4 can enhance the photocatalytic performance.[29] Similarly, N-TiO_2/g-C_3N_4,[30] N-In_2TiO_5/g-C_3N_4,[31] and graphene/g-C_3N_4[32] also exhibited better photocatalytic performance compared with g-C_3N_4. However, the photocatalytic activities of those composites were still low. Therefore, more efficient photocatalytic structures need to be developed.

In this paper, a novel g-C_3N_4/$DyVO_4$ heterostructured photocatalyst was prepared for the first time via a mixing and

Received: July 4, 2012
Revised: October 18, 2012
Accepted: October 24, 2012
Published: October 24, 2012

dx.doi.org/10.1021/ie301774e | *Ind. Eng. Chem. Res.* 2012, 51, 14729−14737

heating method. $DyVO_4$ is reported as an efficient photocatalyst with a small band gap (E_g = 2.3 eV).[34] Meanwhile, $DyVO_4$ has matching conduction and valence bands with g-C_3N_4.[34] The coupling of $DyVO_4$ with g-C_3N_4 can promote both the light response and the electron−hole pair separation; the higher photocatalytic activity is thus expected. Rhodamine B (Rh B), which is famous for its good stability, was used as a model compound to investigate the activities of g-C_3N_4/$DyVO_4$ composite under visible-light irradiation (λ > 420 nm). The performance investigation indicates that the g-C_3N_4/$DyVO_4$ composite catalysts show high photocatalytic activities for RhB photodegradation as well as high photocatalytic stability under visible light.

2. EXPERIMENTAL SECTION

2.1. Catalysts Preparation. NH_4VO_3 (>99%), $Dy(NO_3)_2{\cdot}6H_2O$ (>99%), melamine (99%), tetrabutyl titanate (>99.0%), urea (99%), terephthalic acid (>99.0%), NaOH (>96.0%), benzoquinone (>98.0%), KI (>99.0%), 2-propanol (>99.7%), and ethanol (>99.5%) were purchased commercially and used without further purification.

Pure $DyVO_4$ was prepared by a precipitation method: The starting materials, NH_4VO_3 and $Dy(NO_3)_3$, were separately dissolved in deionized water in a molar ratio of 1:1. Then, the two solutions were mixed to give a yellow precipitate. The pH value of the solution was adjusted to 7 by a solution of NH_3. After being aged at room temperature for 2 h, the deposit was filtered, washed three times by water, dried at 100 °C for 12 h, and calcined at 500 °C for 2 h.

The metal-free g-C_3N_4 powders were synthesized by heating melamine in a muffle furnace. In a typical synthesis run, 6 g of melamine was placed in a semiclosed alumina crucible with a cover. The crucible was heated to 520 °C for 4 h with a heating rate of 10 °C/min. After the reaction, the alumina crucible was cooled to room temperature. Graphitic C_3N_4 was obtained in a powder form.

The $DyVO_4$/g-C_3N_4 composite was prepared by a milling and heating method. The typical procedure was as follows: 0.15 g of $DyVO_4$ and 0.85 g of g-C_3N_4 were mixed and ground in an agate mortar for 20 min. Then, the mixture was calcined at 450 °C for 2 h to obtain the 15 wt % $DyVO_4$/g-C_3N_4 catalyst. Other $DyVO_4$/g-C_3N_4 catalysts with different g-C_3N_4 concentrations were prepared by a similar method.

N-doped TiO_2 was prepared as follows: 8.0 mL of tetrabutyl titanate was dissolved in 48 mL of ethanol to obtain solution A, and 5.65 g urea was dissolved in 8.0 mL of H_2O and 24 mL of ethanol to obtain solution B. Solution B was dropped slowly into solution A under stirring to form a sol. The sol was then transformed into a gel after aging for 12 h. Finally, the gel was dried at 80 °C and calcined at 500 °C for 3 h to obtain a yellow product.

2.2. Characterization. The X-ray diffraction (XRD) characterization of the catalysts was carried out on Philips PW3040/60 X-ray diffractometer, using Cu Kα radiation (40 kV/40 mA) with λ = 0.154 06 nm. N_2 adsorption was measured at 77 K on an Autosorb-1 (Quantachrome Instruments). Thermogravimetry/differential thermal analysis (TG-DTA) was carried out (Netzsch STA449) in a flow of air (20 mL/min) at a heating rate of 10 °C/min. The scanning electron microscopy (SEM) pictures were taken on a field emission scanning electron microscope (Nanoscope IIIa). The transmission electron microscopy (TEM) image was collected with a Hitachi S-4800 transmission electron microscope at an accelerating voltage of 200 kV. The Fourier transform infrared spectroscopy (FT-IR) spectra of the catalysts were recorded on Nicolet NEXUS670 with a resolution of 4 cm^{-1}. The X-ray photoelectron spectroscopy (XPS) measurements were performed with a Quantum 2000 Scanning ESCA Microprobe instrument using Al Kα. The C 1s signal was set to a position of 284.6 eV. The UV−vis diffuse reflectance spectra (DRS) of the catalysts were recorded on Thermo Nicolet Evolution 500 equipped with an integrating sphere using $BaSO_4$ as the background. The photoluminescence (PL) spectra of catalysts were collected on an FLS-920 (Edinbergh Instrument). The light source was a Xe lamp (excitation at 365 nm).

2.3. Photocurrent Measurement. Photocurrent was measured on an electrochemical analyzer (CHI660B) in a standard three-electrode system under zero bias. The prepared sample, a Pt wire, and Ag/AgCl (saturated KCl) are used as the working electrode, the counter electrode, and the reference electrode, respectively. A 500 W Xe arc lamp through a UV-cutoff filter (λ > 420 nm) served as a light source. Na_2SO_4 (0.5 mol/L) aqueous solution was used as the electrolyte. Working electrodes were prepared as follows: An indium tin oxide (ITO) glass piece with a size of 1.5 × 5 cm was cleaned successively by acetone, boiling NaOH (0.1 mol/L), deionized water, and then dried in an air stream. Electrically conductive adhesive with a size of 0.8 × 0.8 cm was pressed on the bottom center of the ITO glass. Finally, the sample powder was ground and closely compacted on the exposed electrically conductive adhesive.

2.4. Photocatalyic Reaction. The photocatalytic activities of the synthesized powders were evaluated by the degradation of RhB by using a spherical Xe lamp (350 W) as light source. Light was passed through two cutoff filters (800 nm > λ > 420 nm) and then was focused onto a 500-mL beaker containing RhB (10 mg/L). The power density at the position of the reactor is about 7.3 mW/cm^2. The volume of the initial RhB solution was 300 mL. All powders contents in the RhB aqueous solution were 0.10 g/100 mL. Prior to irradiation, the mixture was agitated for an hour to ensure adsorption/desorption equilibrium at room temperature. At given irradiation time intervals, 8 mL aliquots were collected and centrifuged to remove the catalyst particulates for analysis. The filtrates were analyzed by recording variations at the wavelength of maximal absorption (554 nm) in the UV−vis spectra of RhB with a UV−vis spectrophotometer. The photocatalytic activities of 15 wt % $DyVO_4$/g-C_3N_4 sample in the photodegradation of methyele blue (MB, 10 mg/L) under visible-light irradiation were also investigated by the same method. Chemical oxygen demand (COD) was measured according to the method presented by Thomas and Mazas,[35] using a dichromate solution as the oxidizing agent in a strong acid medium.

The examination experiment process of reactive species is similar to the photodegradation experiment. A quantity of scavengers was introduced into the RhB solution prior to addition of the catalyst. Terephthalic acid photoluminescence probing technique (TA-PL) is used in the detection of $^{\bullet}OH$ radicals.[36] In the detection experiment, a basic TA solution was added to the reactor instead of RhB, and the concentration of TA was set at 5 × 10^{-3} mol/L in 1 × 10^{-2} mol/L NaOH solution. The $^{\bullet}OH$ formed in the system can react with TA and generate 2-hydroxyterephthalic acid (HTA), the fluorescence intensity of which is directly proportional to the generated $^{\bullet}OH$. The photoluminescence (PL) spectra were collected on

FLS-920 spectrometer (Edinbergh Instrument), using a Xe lamp (excitation at 316 nm) as light source.

3. RESULTS AND DISCUSSION

3.1. Characterizations of the $DyVO_4/g\text{-}C_3N_4$ Composites. Different from the ordinary organic semiconductors, g-C_3N_4 is stable on exposure to oxygen and water,[28] as proven by the TG-DTA experiment shown in Figure 1. Pure g-C_3N_4 is

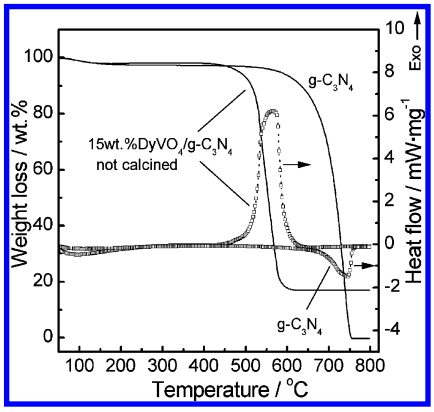

Figure 1. TG-DTA thermograms for heating the pure g-C_3N_4 and the precursor of 15 wt % $DyVO_4/g\text{-}C_3N_4$.

stable in air flow below 600 °C. When the temperature is higher than 600 °C, the sublimation or decomposition of g-C_3N_4 occurred. A sharp weight loss with an endothermal peak at 743 °C was thus observed in the TG-DTA curve of the pure g-C_3N_4. For the $DyVO_4$ and g-C_3N_4 mixture, however, the stability of g-C_3N_4 greatly decreased. The beginning temperature of the weight loss shifted to ca. 440 °C, and the endothermal peak is changed to an exothermal peak. It indicates that the g-C_3N_4 loss in the $DyVO_4/g\text{-}C_3N_4$ mixture can be attributed to the oxidation of g-C_3N_4. This assignment is reasonable considering that $DyVO_4$ has the ability of activating oxygen.[37] Moreover, because the calcination temperature is higher than 440 °C, some g-C_3N_4 might be oxidized to gas product during the heating process. In order to obtain the real g-C_3N_4 concentration, the $DyVO_4/g\text{-}C_3N_4$ composites were characterized by TG-DTA (see Supporting Information, Figure S1). The result is shown in Table 1. The real g-C_3N_4

Table 1. Specific Surface Area and the Real g-C_3N_4 Concentration of $DyVO_4/g\text{-}C_3N_4$ Composite Photocatalysts

catalysts	$S/m^2 \cdot g^{-1}$	concn of g-C_3N_4/wt %
g-C_3N_4	13	100
$DyVO_4$	71	–
10 wt.%$DyVO_4/g\text{-}C_3N_4$	39	88.0
15 wt.%$DyVO_4/g\text{-}C_3N_4$	35	75.0
20 wt.%$DyVO_4/g\text{-}C_3N_4$	32	70.2
30 wt.%$DyVO_4/g\text{-}C_3N_4$	42	66.1
40 wt.%$DyVO_4/g\text{-}C_3N_4$	61	34.7

concentration is lower than the ideal concentration but still maintains the same order. The specific surface areas of $DyVO_4$, g-C_3N_4, and $DyVO_4/g\text{-}C_3N_4$ composites are also shown in Table 1. $DyVO_4$ has much higher BET value than g-C_3N_4, which might be due to the different morphology. As shown in Figure 2, pure $DyVO_4$ is a nanomaterial with an average particle size of approximately 50 nm. For g-C_3N_4, the SEM image

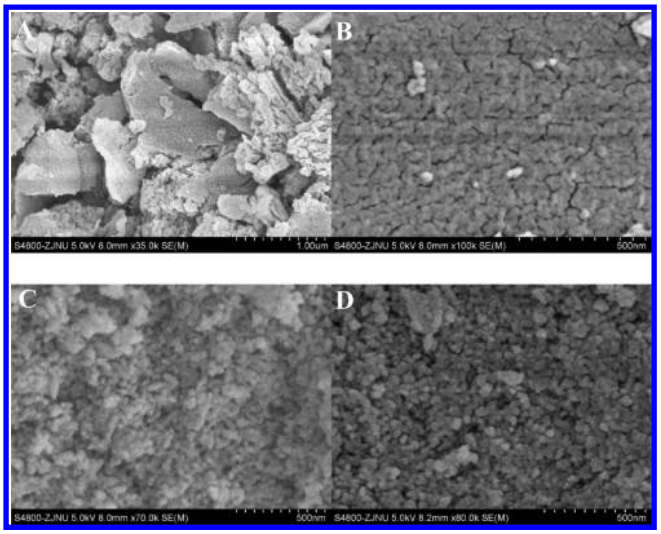

Figure 2. SEM photograph of pure g-C_3N_4 (A, B), $DyVO_4$ (C), and a representative catalyst 15 wt % $DyVO_4/g\text{-}C_3N_4$ (D).

shows that it is also composed of small particles. However, these particles greatly agglomerated, which may be the origin of the low g-C_3N_4 surface area (13 $m^2 \cdot g^{-1}$). The addition of $DyVO_4$ changes the catalyst morphology. As shown in Figure 2D, 15 wt % $DyVO_4/g\text{-}C_3N_4$ sample presents a similar appearance as the pure $DyVO_4$, and a higher specific surface area (35 $m^2 \cdot g^{-1}$) than that of g-C_3N_4 was thus obtained on the sample. The BET surface area of the samples containing 10 and 20 wt % $DyVO_4$ is close to that of the 15 wt % $DyVO_4/g\text{-}C_3N_4$ catalyst. When the $DyVO_4$ concentration is higher than 20 wt %, the BET value of the samples increases with the increasing $DyVO_4$ concentration.

Figure 3 shows the TEM photograph of a representative catalyst, 15 wt % $DyVO_4/g\text{-}C_3N_4$. Two kinds of particles were

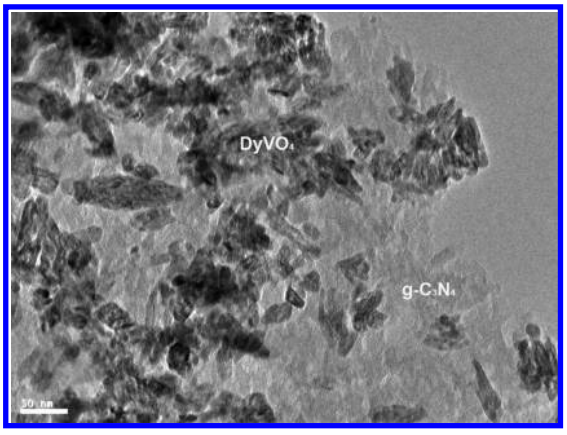

Figure 3. TEM photograph of a representative catalyst, 15 wt % $DyVO_4/g\text{-}C_3N_4$.

observed. The particle with dark color can be assigned to $DyVO_4$ because the electron beam has difficulty passing through the heavy atom, whereas the gray particle can be ascribed to g-C_3N_4. The assignment is verified by the HR-TEM experiment (see Supporting Information, Figure S2). It can be seen that the agglomeration of g-C_3N_4 particle is prevented, and the two kinds of particles disperse finely, which is consistent with the result in Figure 2.

dx.doi.org/10.1021/ie301774e | Ind. Eng. Chem. Res. 2012, 51, 14729−14737

The structure of the $DyVO_4/g\text{-}C_3N_4$ composites was characterized by XRD. Figure 4 shows the XRD patterns of

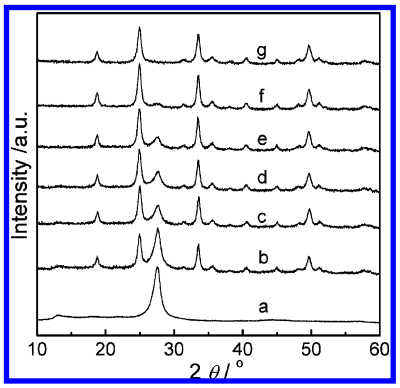

Figure 4. XRD patterns of (a) $g\text{-}C_3N_4$, (g) $DyVO_4$, and $DyVO_4/g\text{-}C_3N_4$ photocatalysts of various concentrations: (b) 10 wt %, (c) 15 wt %, (d) 20 wt %, (e) 30 wt %, and (f) 40 wt %.

$g\text{-}C_3N_4$, $DyVO_4$, and $DyVO_4/g\text{-}C_3N_4$ composite photocatalysts. One strong peak is found in $g\text{-}C_3N_4$ at 27.4°, corresponding to the characteristic interplanar staking peak of aromatic systems.[38] Pure $DyVO_4$ is in its tetragonal phase and exhibits several robust diffraction peaks at 18.7°, 24.9°, 33.5°, and 49.7° (PDF# 16-0870). The $DyVO_4/g\text{-}C_3N_4$ composite presents a two-phase composition: $g\text{-}C_3N_4$ and $DyVO_4$. With the increase in $DyVO_4$ concentration, the $DyVO_4$ peaks strengthened at the expense of that of $g\text{-}C_3N_4$. No impurity was observed. The result in Figure 4 is also verified by the FT-IR experiment. As shown in Figure 5, both of the characteristic peaks of $DyVO_4$

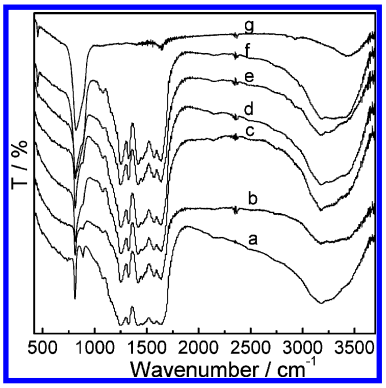

Figure 5. FT-IR spectra of (a) $g\text{-}C_3N_4$, (g) $DyVO_4$, and $DyVO_4/g\text{-}C_3N_4$ photocatalysts of varying concentrations: (b) 10 wt %, (c) 15 wt %, (d) 20 wt %, (e) 30 wt %, and (f) 40 wt %.

(452, 819 cm^{-1}) and those of $g\text{-}C_3N_4$ (1251, 1325, 1419, 1571, and 1639 cm^{-1}) were observed on the $DyVO_4/g\text{-}C_3N_4$ composites, and the peaks' intensity is correlated with their concentrations.

The surface chemical composition and chemical states of $DyVO_4/g\text{-}C_3N_4$ catalysts were analyzed by means of XPS. Figure 6 shows the XPS spectra of $g\text{-}C_3N_4$, $DyVO_4$, and 15 wt % $DyVO_4/g\text{-}C_3N_4$ composite. The XPS spectrum of $DyVO_4/g\text{-}C_3N_4$ composite corresponds exactly to the superposition of those observed for the individual semiconductors (Figure 6A). Both signals of Dy and those of V, C, N, and O were detected. Figure 6B shows the C1s XPS spectra of the above three samples. Only one peak located at 284.6 eV, which is related to carbon contamination, was observed in the $DyVO_4$ sample. For $g\text{-}C_3N_4$ sample, in addition to the polluted carbon peak, another peak at 288.0 eV, which can be assigned to the N−C−N coordination in graphitic carbon nitride, was observed.[39] The 15 wt % $DyVO_4/g\text{-}C_3N_4$ sample also displays two C1s peaks at 284.6 and 288 eV, indicating the existence of $g\text{-}C_3N_4$. However, the peak intensity at 288.0 eV is weaker than that of the $g\text{-}C_3N_4$ sample. A similar phenomenon was also observed in the N1s XPS spectra (Figure 6C), which can be due to the lower concentration of $g\text{-}C_3N_4$ in the 15 wt % $DyVO_4/g\text{-}C_3N_4$ sample. Figure 6D shows the valence-band (VB) XPS spectrum of $g\text{-}C_3N_4$ and $DyVO_4$. The position of the valence band edge of $g\text{-}C_3N_4$ is located at about 1.50 eV, consistent with the result of Yan.[28] For $DyVO_4$, the VB edge is determined to be 1.98 eV.

Figure 7 shows the UV−vis diffuse reflectance spectra of $DyVO_4$, $g\text{-}C_3N_4$, and $DyVO_4/g\text{-}C_3N_4$ composites. For clarity, only 10 and 30 wt % $DyVO_4/g\text{-}C_3N_4$ samples are presented. The UV−vis spectra of other $DyVO_4/g\text{-}C_3N_4$ composites and $N\text{-}TiO_2$ are shown in Figure S3 (Supporting Information). Both $DyVO_4$ and $g\text{-}C_3N_4$ can absorb UV to visible light. The absorption edge of $DyVO_4$ is higher than that of $g\text{-}C_3N_4$, indicating its stronger photoabsorption ability. Correspondingly, $DyVO_4$ (E_g = 2.30 eV) presents a smaller band gap than $g\text{-}C_3N_4$ (E_g = 2.70 eV, Figure 7B). The UV−vis spectra of the $DyVO_4/g\text{-}C_3N_4$ composite samples can be seen as the overlap of that of the $DyVO_4$ and $g\text{-}C_3N_4$. With the increase in the $DyVO_4$ concentration, the characteristic peak of $DyVO_4$ (307 nm) increases at the expense of the peak of $g\text{-}C_3N_4$ (382 nm), consistent with the XRD and FT-IR results. However, because of the low content of $DyVO_4$ and weak light absorbency of $DyVO_4$ in the range of 400−500 nm, all $DyVO_4/g\text{-}C_3N_4$ composites display a similar absorption edge as the pure $g\text{-}C_3N_4$, suggesting that addition of $DyVO_4$ slightly changed the optical properties. $N\text{-}TiO_2$ exhibits the highest photoabsorption performance (Supporting Information, Figure S3).

3.2. Photocatalytic Activity of the $DyVO_4/g\text{-}C_3N_4$ Composites. The photocatalytic activity of $DyVO_4/g\text{-}C_3N_4$ composites was evaluated by decomposing RhB under visible-light irradiation (λ> 420 nm). Figure 8 shows the photocatalytic activity of the $DyVO_4/g\text{-}C_3N_4$ composite photocatalysts with different $DyVO_4$ concentrations. As seen in Figure 8A, without a catalyst the absorbency of RhB solution displays little difference before and after the visible-light illumination from a 350 W xenon lamp for 2 h. It can be concluded that the RhB is stable under the experimental conditions. N-doped TiO_2 is usually considered as an effective visible-light-driven photocatalyst. In Figure 8A, its photocatalytic activity is higher than that of $DyVO_4$ but lower than that of $g\text{-}C_3N_4$. For $DyVO_4/g\text{-}C_3N_4$ composite samples, the photocatalytic activity is greatly influenced by the $DyVO_4$ concentration. With the increase in the $DyVO_4$ concentration, the photocatalytic activity first increases and then decreases. The 15 wt % $DyVO_4/g\text{-}C_3N_4$ sample has the optimal photocatalytic activity. The corresponding first-order kinetics plot shown in Figure 8B indicates that the 15 wt % $DyVO_4/g\text{-}C_3N_4$ composite exhibits the highest degradation rate of 2.190 h^{-1}, which is 10.3, 5.3, and 2.6 times higher than that of $DyVO_4$, $N\text{-}TiO_2$, and $g\text{-}C_3N_4$, respectively. Chemical oxygen demand (COD) measurements of the RhB solution were also carried out to verify whether dye decolorization is accomplished with its degradation. The result shows a COD removal of 96.0% during the photoirradiation process, suggesting that the 15 wt % $DyVO_4/g\text{-}C_3N_4$ sample presents a strong ability in complete oxidation (see Supporting Information, Figure S4). Of course, the rate of the

dx.doi.org/10.1021/ie301774e | Ind. Eng. Chem. Res. 2012, 51, 14729−14737

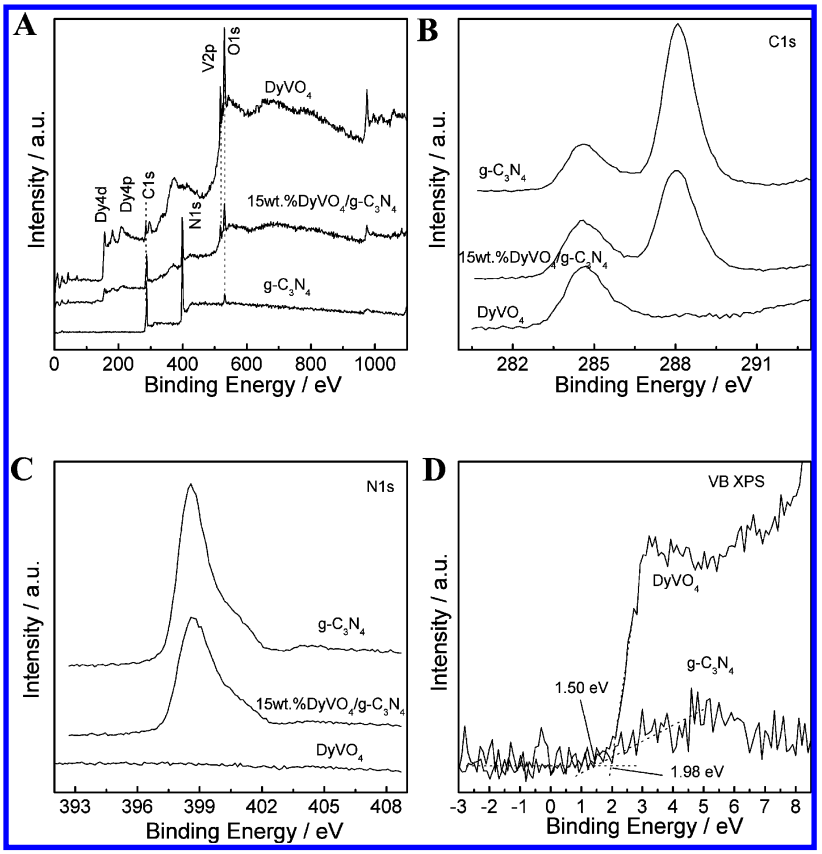

Figure 6. (A) XPS spectra of g-C_3N_4, $DyVO_4$, and 15 wt % $DyVO_4$/g-C_3N_4 composite and (B) C1s, (C) N1s, and (D) valence band XPS.

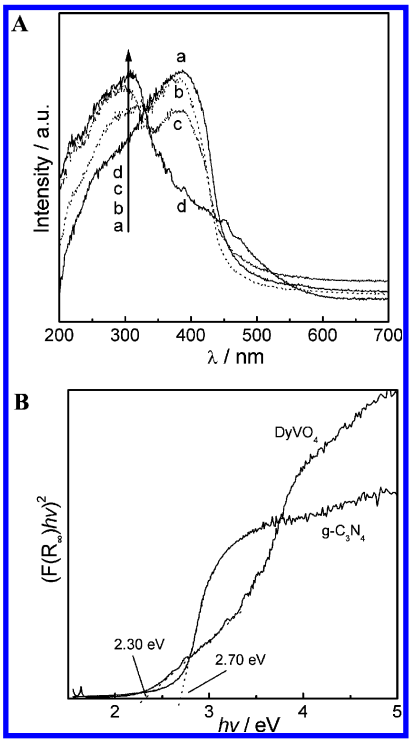

Figure 7. UV−vis spectra (A) of (a) g-C_3N_4, (d) $DyVO_4$, and (b) 15 wt % and (d) 40 wt % $DyVO_4$/g-C_3N_4 photocatalysts and (B) estimated band gap of photocatalyst by the Kubelka−Munk function.

decolorization is slightly higher than that of COD removal over the 15 wt % $DyVO_4$/g-C_3N_4 sample, indicating there are still some organic fragments in solution. The same phenomenon was also observed over the P25 and N-TiO_2 photocatalysts.

In order to investigate the reusable stability of $DyVO_4$/g-C_3N_4 composite photocatalysts, the recycling experiments on 15 wt % $DyVO_4$/g-C_3N_4 sample were also carried out under the same reaction conditions. The catalyst was separated from the reaction mixture by centrifugation after each reaction cycle. The result in Figure 9 indicates that the 15 wt % $DyVO_4$/g-C_3N_4 sample possesses durable high photocatalytic activity after the RhB photodegradation reaction was repeated five times. In addition to RhB degradation, the $DyVO_4$/g-C_3N_4 composite also shows high photocatalytic activity for methylene blue (MB) degradation (see Supporting Information, Figure S5). Compared with RhB, the dye-sensitization effect of MB is poor. That is why the photoactivity of P25 in MB degradation is much lower than that in RhB degradation under visible-light irradiation. The result in Figure S5 (Supporting Information) clearly indicates that the high VLD photoactivity of $DyVO_4$/g-C_3N_4 composite mainly originates from the coupled system itself.

3.3. Discussion. The composite photocatalysts have attracted increasing attention for their enhanced performance. Some researchers attribute the increased activity to the adsorption ability for the organic compounds, which are often related to the specific surface area.[40] In the present work, however, no consistent correlation between the BET area and the photocatalytic activity was observed. It suggests that the adsorption ability of $DyVO_4$/g-C_3N_4 catalysts shows little effect on the photocatalytic activity. The key factor impacting the catalytic activity might be the composition of the catalysts themselves.

dx.doi.org/10.1021/ie301774e | Ind. Eng. Chem. Res. 2012, 51, 14729−14737

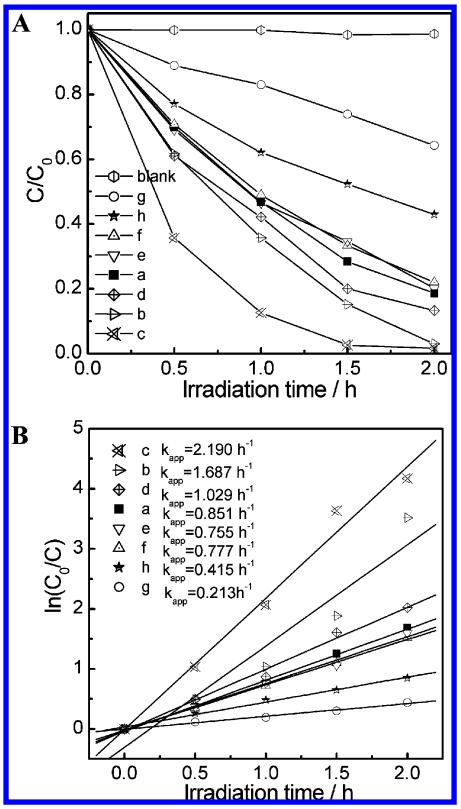

Figure 8. Photocatalytic activity of the $DyVO_4/g\text{-}C_3N_4$ composite photocatalysts for the RhB photodegradation under visible-light irradiation (A) and the corresponding first-order kinetics plot (B) of (a) $g\text{-}C_3N_4$, (b) 10 wt % $DyVO_4/g\text{-}C_3N_4$, (c) 15 wt % $DyVO_4/g\text{-}C_3N_4$, (d) 20 wt % $DyVO_4/g\text{-}C_3N_4$, (e) 30 wt % $DyVO_4/g\text{-}C_3N_4$, (f) 40 wt % $DyVO_4/g\text{-}C_3N_4$, (g) $DyVO_4$, and (h) $N\text{-}TiO_2$.

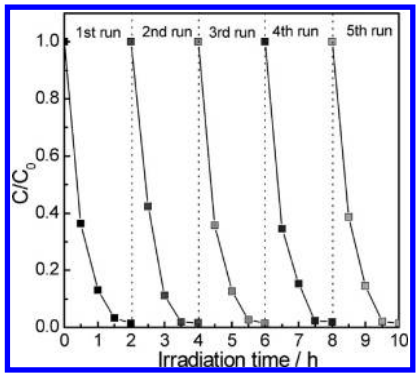

Figure 9. Cycling runs for the photocatalytic degradation of RhB in the presence of 15 wt % $DyVO_4/g\text{-}C_3N_4$ sample under visible light irradiation.

Actually, it is well-known that the photocatalytic activity of photocatalyst mainly depends on whether the electron−hole pairs can be separated effectively. For composite photocatalyst, the enhancement in the separation of charge carriers is usually attributed to the charge transfer at the heterojunction interfaces, which originates from matching band potentials between two semiconductors. The VB edges of $DyVO_4$ and $g\text{-}C_3N_4$ were determined to be 1.98 and 1.50 eV via the VB XPS experiment, respectively. The CB edge potentials of the two semiconductors were thus obtained by using the equation of $E_{CB} = E_{VB} - E_g$. The result is shown in Figure 10. As seen from this figure, $g\text{-}C_3N_4$ displays more negative CB edge potential

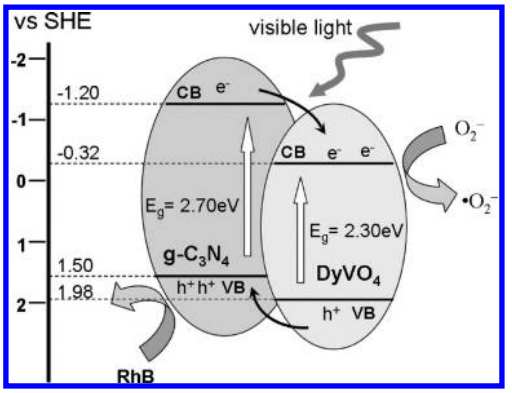

Figure 10. Scheme for electron−hole separation and transport at the visible-light-driven $DyVO_4/g\text{-}C_3N_4$ composite photocatalyst interface.

than $DyVO_4$, indicating that the photogenerated electrons on $g\text{-}C_3N_4$ particle surfaces can transfer easily to $DyVO_4$. Meanwhile, the photoinduced holes on the $DyVO_4$ surface can move to $g\text{-}C_3N_4$ due to the large difference in VB edge potentials. This charge transfer reduces the probability of electron−hole recombination and leads to a larger amount of electrons on the $DyVO_4$ surface and holes on the $g\text{-}C_3N_4$ surface, respectively, which promote the photocatalytic reactions to decompose RhB.

In order to prove the above-proposed suggestion about the electron−hole separation, the $DyVO_4/g\text{-}C_3N_4$ composite was characterized by PL, which can reveal the migration, transfer, and recombination processes of photogenerated electron−hole pairs in semiconductors.[29,34,41] Figure 11 shows the PL spectra

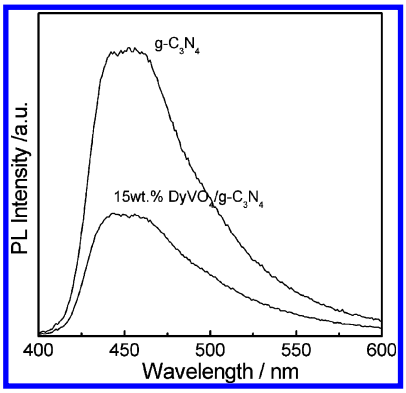

Figure 11. Photoluminescence spectra of pure $g\text{-}C_3N_4$ and $DyVO_4/g\text{-}C_3N_4$ composite.

of the 15 wt % $DyVO_4/g\text{-}C_3N_4$ composite photocatalysts at an excitation wavelength of 365 nm. Pure $g\text{-}C_3N_4$ has a strong emission band centered at 460 nm, which can be attributed to the radiative recombination process of self-trapped excitations.[29] The PL spectrum of $DyVO_4/g\text{-}C_3N_4$ composite is similar to that of pure $g\text{-}C_3N_4$, but its peak intensity is much lower. Because PL emission results from the recombination of free charge carriers, the result in Figure 11 clearly indicates that the recombination of photogenerated charge carriers is inhibited in the $DyVO_4/g\text{-}C_3N_4$ composite semiconductors.

The photocurrent−time measurement was used to further elucidate the interfacial charge transfer dynamics between the interfacial surface of $DyVO_4$ and $g\text{-}C_3N_4$ semiconductors. The photocurrent is widely regarded as the most efficient evidence to demonstrate the charge separation in composite photo-

dx.doi.org/10.1021/ie301774e | Ind. Eng. Chem. Res. 2012, 51, 14729−14737

catalysts.[42] The photocurrent value represents the charge collection efficiency. A relationship is commonly recognized: the higher the photocurrent is, the higher the e^-−h^+ separation efficiency is, which is beneficial for the photocatalytic reaction. Figure 12 shows the photocurrent−time curves of g-C_3N_4, $DyVO_4$, and 15 wt % $DyVO_4$/g-C_3N_4 composite with two on−off cycles of intermittent irradiation. The electrodes of the three samples are prompt in generating photocurrent with a reproducible response to on−off cycles. The 15 wt % $DyVO_4$/g-C_3N_4 composite sample presents a photocurrent of 0.93 μA, which is much higher than that of g-C_3N_4 and $DyVO_4$. This result indicates the suppression of the charge recombination process in the $DyVO_4$/g-C_3N_4 heterojunction, as proven by the PL analysis.

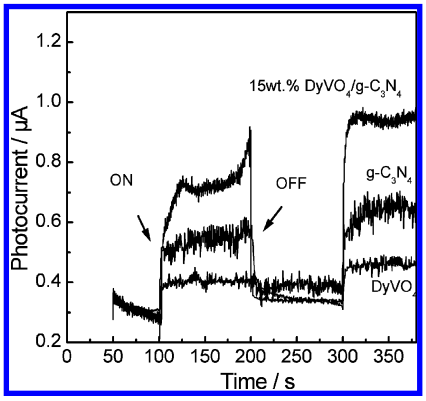

Figure 12. Transient photocurrent response for $DyVO_4$, g-C_3N_4, and 15 wt % $DyVO_4$/g-C_3N_4 samples.

Therefore, it is clearly that the charge transfer exists in the $DyVO_4$/g-C_3N_4 heterojunction, which results in an accumulation of photogenerated electrons on the $DyVO_4$ CB and holes on the g-C_3N_4 VB. The electrons in $DyVO_4$ are good reductants that could capture O_2 and reduce it to $^\bullet O_2^-$ since the CB edge potential of $DyVO_4$ is more negative than $E_{O_2/^\bullet O_2^-}$ (−0.28 V vs SHE).[4] This inference has been proven before. The $^\bullet O_2^-$ species was detected by electron spin-resonance spectroscopy (ESR) on photocatalyst $BiVO_4$ whose CB edge potential is slightly more positive than that of $DyVO_4$.[34,43−45] The further reduction of $^\bullet O_2^-$ can lead to the formation of $^\bullet$OH. Actually, it is reported that the oxidative species $^\bullet$OH can also be generated by the reaction of h^+ with H_2O.[4,46] In the $DyVO_4$/g-C_3N_4 composite, however, the reaction cannot occur because of the low VB edge potential of g-C_3N_4 ($E_{^\bullet OH/H_2O}$ = 2.27 V vs SHE).[4] $^\bullet O_2^-$, h^+, and $^\bullet$OH are suspected to be involved in the photocatalytic oxidation process.[39] In order to evaluate the role of the three reactive species, different scavenges used as probes are introduced into the photocatalytic degradation of RhB. The dosages are from previous studies.[46,47] As Figure 13 showed, the degradation rate (k_{app}) decreases obviously to 0.038 h^{-1} in the presence of benzoquinone (BQ, $^\bullet O_2^-$ scavenger), which suggests that $^\bullet O_2^-$ is the main reactive species for RhB degradation. The addition of KI (h^+ and $^\bullet$OH quencher) also leads to a great decrease in photocatalytic activity. Meanwhile, 2-propanol (IPA, a quencher of $^\bullet$OH) shows little effect on the k_{app} of RhB. It suggests that h^+ is also an important reactive species besides $^\bullet O_2^-$ species. The TA-PL probing measurement was carried out to further study the role of •OH species. Figure 14 shows the •OH-trapping photoluminescence spectra of g-C_3N_4, $DyVO_4$, and 15 wt % $DyVO_4$/g-C_3N_4 composite under visible-light irradiation. PL emission peak at 426 nm was observed in all samples, indicating the generation of $^\bullet$OH species. However, the peak intensity of $DyVO_4$/g-C_3N_4 composite is lower than that of g-C_3N_4 and $DyVO_4$, which is inconsistent with their photocatalytic activities. This result indicates that the generated $^\bullet$OH species is not the main reactive species, as shown in Figure 13. On the basis of the analysis above, a possible mechanism for the photocatalytic oxidation of RhB on $DyVO_4$/g-C_3N_4 composite is suggested. The process is described as follows:

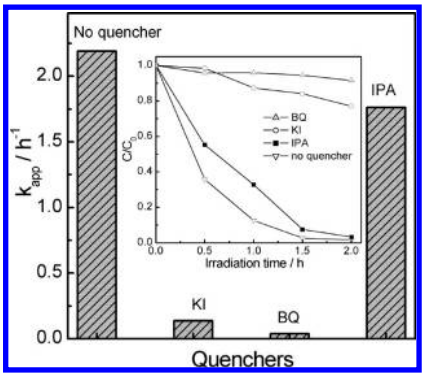

Figure 13. k_{app}-Values and photocatalytic activity of $DyVO_4$/g-C_3N_4 photocatlalysts with different quenchers.

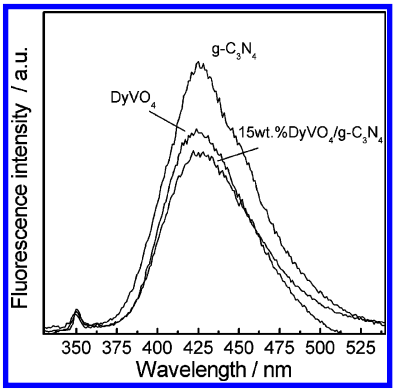

Figure 14. $^\bullet$OH-trapping photoluminescence spectra of photocatalyst under visible-light irradiation in a solution of terephthalic acid at room temperature.

$$DyVO_4/g\text{-}C_3N_4 \xrightarrow{h\nu} DyVO_4(e^- + h^+)/g\text{-}C_3N_4(e^- + h^+) \quad (1)$$

$$DyVO_4(e^- + h^+)/g\text{-}C_3N_4(e^- + h^+) \rightarrow DyVO_4(e^-)/g\text{-}C_3N_4(h^+) \quad (2)$$

$$O_2 + e^- \rightarrow {}^\bullet O_2^- \quad (3)$$

$$^\bullet O_2^- + 2H^+ + e^- \rightarrow H_2O_2 \quad (4)$$

$$H_2O_2 + e^- \rightarrow {}^\bullet OH + OH^- \quad (5)$$

$$^\bullet O_2^-/h^+ + RhB \rightarrow \text{degradation pruducts} \quad (6)$$

Although $DyVO_4$ greatly promotes the photocatalytic activity of g-C_3N_4, the promotion effect is not the highest compared with the other dopers. The improvement is higher than that of N-TiO_2 and TaON, but lower than that of Bi_2WO_6 based on

dx.doi.org/10.1021/ie301774e | Ind. Eng. Chem. Res. 2012, 51, 14729−14737

the literatures reported.[28−32] However, it should be noted that the doping amount of $DyVO_4$ is the lowest, which decreases the cost of the synthesized photocatalyst. In addition, the $DyVO_4$/g-C_3N_4 exhibits a strong ability in complete oxidation. Both of the above-mentioned points are beneficial for the application of $DyVO_4$/g-C_3N_4 catalyst on a large scale. Moreover, the successful doping of $DyVO_4$ suggests that other cheaper vanadates (such as $LaVO_4$, $BiVO_4$) might also promote the photoactivity of g-C_3N_4. It is believed that the developed vandates/g-C_3N_4 photocatalyst would hold the advantages of both high activity and low cost and is promising in practical applications in water purification.

4. CONCLUSIONS

In summary, we have prepared a novel $DyVO_4$/g-C_3N_4 composite photocatalyst by the milling and heating method. The stable dye RhB was selected as a substrate to evaluate the photocatalytic activity of $DyVO_4$/g-C_3N_4. Our results clearly indicate that the synthesized composite has good performance. The highest degradation efficiency was achieved for the 15 wt % $DyVO_4$/g-C_3N_4 sample. On the basis of the energy band positions, PL spectra, and PC curves, the enhanced photocatalytic activity is attributed to the synergy effect between $DyVO_4$ and g-C_3N_4.

■ ASSOCIATED CONTENT

Ⓢ Supporting Information

TG-DTA thermograms for heating the $DyVO_4$/g-C_3N_4 composites (Figure S1); HR-TEM of 15 wt % $DyVO_4$/g-C_3N_4 composite (Figure S2); UV−vis spectra of g-C_3N_4, N-TiO_2, and $DyVO_4$/g-C_3N_4 composites (Figure S3); COD removal of 15 wt % $DyVO_4$/g-C_3N_4, N-TiO_2, and P25 photocatalysts (Figure S4); photocatalytic activity of MB and RhB over 15 wt % $DyVO_4$/g-C_3N_4, N-TiO_2, and P25 photocatalysts (Figure S5). This material is available free of charge via the Internet at http://pubs.acs.org/.

■ AUTHOR INFORMATION

Corresponding Author

*Tel: +86-0579-83792294. Fax: +86-0579-83714946. E-mail: hym@zjnu.cn.

Notes

The authors declare no competing financial interest.

■ ACKNOWLEDGMENTS

This work was supported by the National Natural Science Foundation of China (No. 21003109) and the program for Changjiang Scholars and Innovative Research Team in Chinese Universities (No. IRT0980).

■ REFERENCES

(1) Chong, M. N.; Jin, B.; Chow, C. W. K.; Saint, C. Recent developments in photocatalytic water treatment technology: A review. *Water Res.* **2010**, *44*, 2997−3027.

(2) Chen, X. B.; Shen, S. H.; Guo, L. J.; Mao, S. S. Semiconductor-based photocatalytic hydrogen generation. *Chem. Rev.* **2010**, *110*, 6503−6570.

(3) Malato, S.; J. Blanco, J.; Vidal, A.; Richter, C. Photocatalysis with solar energy at a pilot-plant scale: An overview. *Appl. Catal., B* **2002**, *37*, 1−15.

(4) Fujishima, A.; Rao, T. N.; Tryk, D. A. Titanium dioxide photocatalysis. *J. Photochem. Photobiol., C* **2000**, *1*, 1−21.

(5) Choi, W.; Termin, A.; Hoffmann, M. R. The role of metal ion dopants in quantum-sized TiO_2: Correlation between photoreactivity and charge carrier recombination dynamics. *J. Phys. Chem.* **1994**, *98*, 13669−13679.

(6) Yamashita, H.; Harada, M.; Misaka, J.; Takeuchi, M.; Ikeue, K.; Anpo, M. Degradation of propanol diluted in water under visible light irradiation using metal ion-implanted titanium dioxide photocatalysts. *J. Photochem. Photobiol., A* **2002**, *148*, 257−261.

(7) Ashi, R.; Morikawa, T.; Ohwaki, T.; Aoki, K.; Taga, Y. Visible-light photocatalysis in nitrogen-doped titanium oxides. *Science* **2001**, *293*, 269−271.

(8) Sakthivel, S.; Kisch, H. Daylight photocatalysis by carbon-modified titanium dioxide. *Angew. Chem., Int. Ed.* **2003**, *42*, 4908−4911.

(9) Gordon, T. R.; Cargnello, M.; Paik, T.; Mangolini, F.; Weber, R. T.; Fornasiero, P.; Murray, C. B. Nonaqueous synthesis of TiO_2 nanocrystals using TiF_4 to engineer morphology, oxygen vacancy concentration, and photocatalytic activity. *J. Am. Chem. Soc.* **2012**, *134*, 6751−6761.

(10) Chen, X. B.; Liu, L.; Yu, P. Y.; Mao, S. S. Increasing solar absorption for photocatalysis with black hydrogenated titanium dioxide nanocrystals. *Science* **2011**, *331*, 746−750.

(11) Qin, G. H.; Sun, Z.; Wu, Q. P.; Lin, L.; Liang, M.; Xue, S. Dye-sensitized TiO_2 film with bifunctionalized zones for photocatalytic degradation of 4-cholophenol. *J. Hazard. Mater.* **2011**, *192*, 599−604.

(12) Zhang, L.; He, Y. M.; Wu, Y.; Wu, T. H. Photocatalytic degradation of RhB over $MgFe_2O_4/TiO_2$ composite materials. *Mater. Sci. Eng., B* **2011**, *176*, 1497−1504.

(13) Sun, M.; Chen, G. D.; Zhang, Y. K.; Wei, Q.; Ma, Z. M.; Du, B. Efficient degradation of azo dyes over Sb_2S_3/TiO_2 heterojunction under visible light irradiation. *Ind. Eng. Chem. Res.* **2012**, *51*, 2897−2903.

(14) Sun, S. M.; Wang, W. Z.; Zhou, L.; Xu, H. L. Efficient methylene blue removal over hydrothermally synthesized starlike $BiVO_4$. *Ind. Eng. Chem. Res.* **2009**, *48*, 1735−1739.

(15) Bi, Y. P.; Ouyang, S. X.; Umezawa, N.; Cao, J. Y.; Ye, J. H. Facet effect of single-crystalline Ag_3PO_4 sub-microcrystals on photocatalytic properties. *J. Am. Chem. Soc.* **2011**, *133*, 6490−6492.

(16) Wang, Y. J.; He, Y. M.; Li, T. T.; Cai, J.; Luo, M. F.; Zhao, L. H. Photocatalytic degradation of methylene blue on $CaBi_6O_{10}/Bi_2O_3$ composites under visible light. *Chem. Eng. J.* **2012**, *189−190*, 473−481.

(17) Bai, X. D.; Zhong, D. Y.; Zhang, G. Y.; Ma, X. C.; Liu, S.; Wang, E. G.; Chen, Y.; Shaw, D. T. Hydrogen storage in carbon nitride nanobells. *Appl. Phys. Lett.* **2001**, *79*, 1552−1554.

(18) Zhang, Z.; Leinenweber, K.; Bauer, M.; Garvie, L. A. J.; Mcmillan, P. F.; Wolf, G. H. High-pressure bulk synthesis of crystalline $C_6N_9H_3$:HCl: A novel C_3N_4 graphitic derivative. *J. Am. Chem. Soc.* **2001**, *123*, 7788−7796.

(19) Zhang, Y. J.; Mori, T.; Ye, J. H.; Antonietti, M. Phosphorus-doped carbon nitride solid: Enhanced electrical conductivity and photocurrent generation. *J. Am. Chem. Soc.* **2010**, *132*, 6294−6295.

(20) Wang, X. C.; Maeda, K.; Thomas, A.; Takanabe, K.; Xin, G.; Carlsson, J. M.; Domen, K.; Antonietti, M. A metal-free polymeric photocatalyst for hydrogen production from water under visible light. *Nat. Mater.* **2009**, *8*, 76−80.

(21) Yan, S. C.; Li, Z. S.; Zou, Z. G. Photodegradation performance of g-C_3N_4 fabricated by directly heating melamine. *Langmuir* **2009**, *25*, 10397−10401.

(22) Zhang, Y. J.; Mori, T.; Ye, J. H. Polymeric carbon nitrides: Semiconducting properties and emerging applications in photocatalysis and photoelectrochemical energy conversion. *Sci. Adv. Mater.* **2012**, *4*, 282−291.

(23) Ge, L.; Han, C. C.; Liu, J.; Li, Y. F. Enhanced visible light photocatalytic activity of novel polymeric g-C_3N_4 loaded with Ag nanoparticles. *Appl. Catal., A* **2011**, *409−410*, 215−222.

(24) Liu, G.; Niu, P.; Sun, C. H.; Smith, S. C.; Chen, Z. G.; Lu, G. Q.; Cheng, H. M. Unique electronic structure induced high photoreactivity of sulfur-doped graphitic C_3N_4. *J. Am. Chem. Soc.* **2010**, *132*, 11642−11648.

(25) Goettmann, F.; Fischer, A.; Antonietti, M.; Thomas, A. Chemical synthesis of mesoporous carbon nitrides using hard templates and their use as a metal-free catalyst for friedel−crafts reaction of benzene. *Angew. Chem., Int. Ed.* **2006**, *45*, 4467−4471.
(26) Kailasam, K.; Epping, J. D.; Thomas, A.; Losse, S.; Junge, H. Mesoporous carbon nitride−silica composites by a combined sol−gel/thermal condensation approach and their application as photocatalysts. *Energy Environ. Sci.* **2011**, *4*, 4668−4674.
(27) Zhang, Y. J.; Thomas, A.; Antonietti, M.; Wang, X. C. Activation of carbon nitride solids by protonation: Morphology changes, enhanced ionic conductivity, and photoconduction experiments. *J. Am. Chem. Soc.* **2009**, *131*, 50−51.
(28) Yan, S. C.; Lv, S. B.; Li, Z. S.; Zou, Z. G. Organic−inorganic composite photocatalyst of g-C_3N_4 and TaON with improved visible light photocatalytic activities. *Dalton Trans.* **2010**, *39*, 1488−1491.
(29) Ge, L.; Han, C. C.; Liu, J. Novel visible light-induced g-C_3N_4/Bi_2WO_6 composite photocatalysts for efficient degradation of methyl orange. *Appl. Catal., B* **2011**, *108−109*, 100−107.
(30) Yang, N.; Li, G. Q.; Wang, W. L.; Yang, X. L.; Zhang, W. F. Photophysical and enhanced daylight photocatalytic properties of N-doped TiO_2/g-C_3N_4 composites. *J. Phys. Chem. Solid* **2011**, *72*, 1319−1324.
(31) Liu, Y.; Chen, G.; Zhou, C.; Hu, Y. D.; Fu, D. G.; Liu, J.; Wang, Q. Higher visible photocatalytic activities of nitrogen doped In_2TiO_5 sensitized by carbon nitride. *J. Hazard. Mater.* **2011**, *190*, 75−80.
(32) Zhang, Y. J.; Mori, T.; Niu, L.; Ye, J. H. Non-covalent doping of graphitic carbon nitride polymer with graphene: Controlled electronic structure and enhanced optoelectronic conversion. *Energy Environ. Sci.* **2011**, *4*, 4517−4521.
(33) Ang, T. P.; Chan, Y. M. Comparison of the melon nanocomposites in structural properties and photocatalytic activities. *J Phys. Chem. C* **2011**, *115*, 15965−1597.
(34) He, Y. M.; Zhao, L. H.; Wang, Y. J.; Lin, H. J.; Li, T. T.; Wu, X. T.; Wu, Y. Synthesis, characterization and photocatalytic performance of $VDyO_x$ composite under visible light irradiation. *Chem. Eng. J.* **2011**, *169*, 50−57.
(35) Ministry of Environmental Protection of People's Republic of China. *Standard Methods for the Determination of Water and Wastewater*, 4th ed.; China Environmental Science Press: Beijing, 2002; pp 211−213 (in Chinese).
(36) Yan, T. J.; Li, L. P.; Li, G. S.; Wang, Y. J.; Hu, W. B.; Guan, X. F. Porous $SnIn_4S_8$ microspheres in a new polymorph that promotes dyes degradation under visible light irradiation. *J. Hazard. Mater.* **2011**, *186*, 272−279.
(37) Fang, Z. M.; Hong, Q.; Zhou, Z. H.; Dai, S. J.; Weng, W. Z.; Wan, H. L. Oxidative dehydrogenation of propane over a series of low-temperature rare earth orthovanadate catalysts prepared by the nitrate method. *Catal. Lett.* **1999**, *61*, 39−44.
(38) Liao, G. Z.; Chen, S.; Quan, X.; Yu, H. T.; Zhao, H. M. Graphene oxide modified g-C_3N_4 hybrid with enhanced photocatalytic capability under visible light irradiation. *J. Mater. Chem.* **2012**, *22*, 2721−2726.
(39) Yan, H. J.; Chen, Y.; Xu, S. M. Synthesis of graphitic carbon nitride by directly heating sulfuric acid treated melamine for enhanced photocatalytic H_2 production from water under visible light. *Int. J. Hydrogen Energy* **2012**, *37*, 125−133.
(40) Rachel, A.; Sakakha, M.; Subrahmanyam, M.; Boule, P. Comparison of several titanium dioxides for the photocatalytic degradation of benzenesulfonic acids. *Appl. Catal., B* **2002**, *37*, 293−300.
(41) Li, X. Z.; Li, F. B.; Yang, C. L.; Ge, W. K. Photocatalytic activity of WO_x−TiO_2 under visible light irradiation. *J. Photochem. Photobiol., A* **2001**, *141*, 209−217.
(42) Kong, M.; Li, Y. Z.; Chen, X.; Tian, T. T.; Fang, P. F.; Zheng, F.; Zhao, X. J. Tuning the relative concentration ratio of bulk defects to surface defects in TiO_2 nanocrystals leads to high photocatalytic efficiency. *J. Am. Chem. Soc.* **2011**, *133*, 16414−16417.
(43) Long, M. C.; Cai, W. M.; Cai, J.; Zhou, B. X.; Chai, X. Y.; Wu, Y. H. Efficient photocatalytic degradation of phenol over Co_3O_4/$BiVO_4$ composite under visible light irradiation. *J. Phys. Chem. C* **2006**, *110*, 20211−20216.
(44) Zhou, B.; Zhao, X.; Liu, H. J.; Qu, J. H.; Huang, C. P. Synthesis of visible-light sensitive M−$BiVO_4$ (M = Ag, Co, and Ni) for the photocatalytic degradation of organic pollutants. *Sep. Purif. Technol.* **2011**, *77*, 275−282.
(45) Zhao, W. R.; Wang, Y.; Yang, Y.; Tang, J.; Yang, Y. N. Carbon spheres supported visible-light-driven CuO−$BiVO_4$ heterojunction: Preparation, characterization, and photocatalytic properties. *Appl. Catal. B* **2012**, *115−116*, 90−99.
(46) Li, G. T.; Wong, K. H.; Zhang, X. W.; Hu, C.; Yu, J. C.; Chan, R. C. Y.; Wong, P. K. Degradation of Acid Orange 7 using magnetic AgBr under visible light: The roles of oxidizing species. *Chemosphere* **2009**, *76*, 1185−1191.
(47) Lin, H. L.; Cao, J.; Luo, B. D.; Xu, B. Y.; Chen, S. F. Synthesis of novel Z-scheme AgI/Ag/AgBr composite with enhanced visible light photocatalytic activity. *Catal. Commun.* **2012**, *21*, 91−95.